CubeSense++: Smart Environment Sensing with Interaction-Powered Corner Reflector Mechanisms

Xiaoying Yang
University of California, Los Angeles
Los Angeles, CA, USA
xiaoyingy@ucla.edu

Jacob Sayono
University of California, Los Angeles
Los Angeles, CA, USA
jacobsayono@ucla.edu

Yang Zhang
University of California, Los Angeles
Los Angeles, CA, USA
yangzhang@ucla.edu

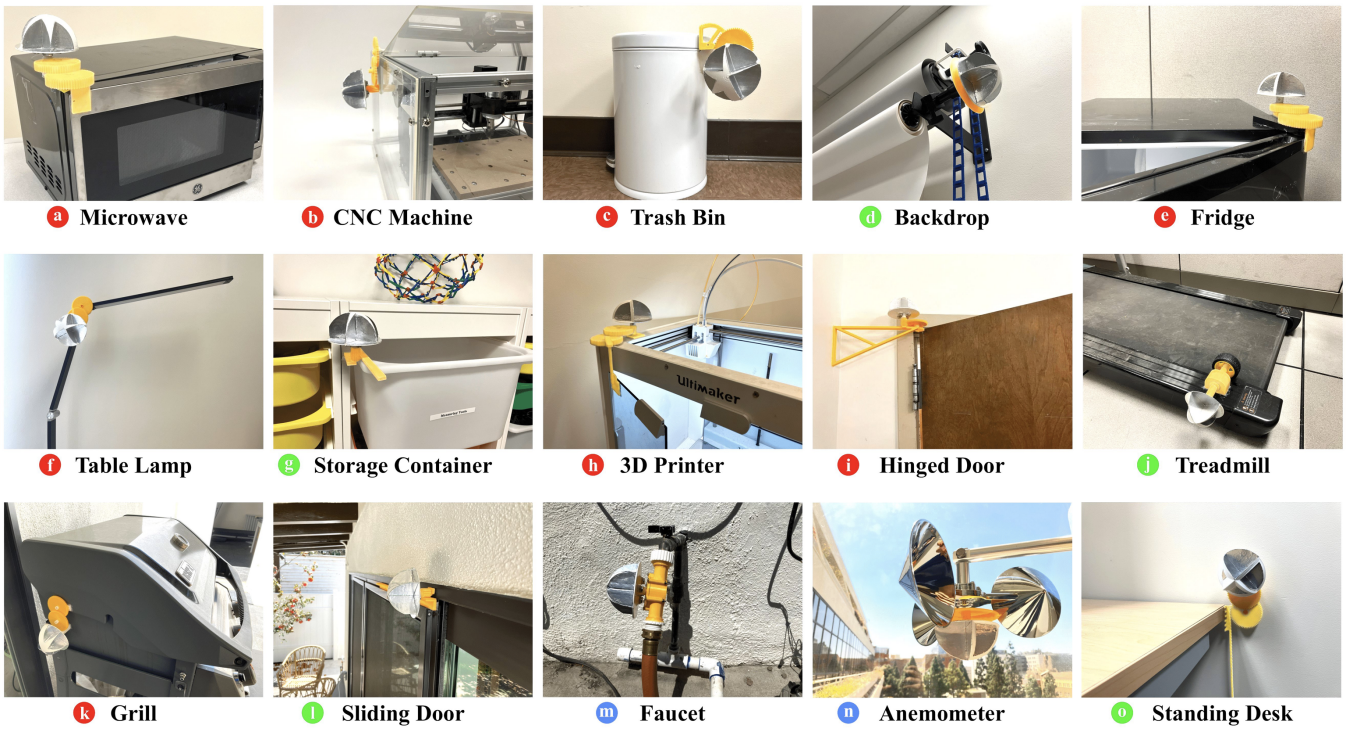

Figure 1: Reflector mechanisms. Red: rotational motion. Green: translational motion. Blue: flow motion.

ABSTRACT

Smart environment sensing provides valuable contextual information by detecting occurrences of events such as human activities and changes of object status, enabling computers to collect personal and environmental informatics to perform timely responses to user's needs. Conventional approaches either rely on tags that require batteries and frequent maintenance, or have limited detection capabilities bounded by only a few coarsely predefined activities. In response, this paper explores corner reflector mechanisms that encode user interactions with everyday objects into structured responses to millimeter wave radar, which has the potential for integration into smart environment entities such as speakers, light bulbs, thermostats, and autonomous vehicles. We presented the design space of 3D printed reflectors and gear mechanisms, which are low-cost, durable, battery-free, and can retrofit to a wide array of objects. These mechanisms convert the kinetic energy from user interactions into rotational motions of corner reflectors which we computationally designed with a genetic algorithm. We built an end-to-end radar detection pipeline to recognize fine-grained activity information such as state, direction, rate, count, and usage based on the characteristics of radar responses. We conducted studies for multiple instrumented objects in both indoor and outdoor environments, with promising results demonstrating the feasibility of the proposed approach.

UIST '23, October 29-November 1, 2023, San Francisco, CA, USA

ACM ISBN 979-8-4007-0132-0/23/10.
https://doi.org/10.1145/3586183.3606744

CCS CONCEPTS

• **Hardware → Sensors and actuators**; **Sensor applications and deployments**; • **Human-centered computing → Human computer interaction (HCI)**.

KEYWORDS

Smart Environment, Millimeter Wave Sensing, Digital Fabrication, Interaction-Powered, Backscatters, Corner Reflectors;

ACM Reference Format:

Xiaoying Yang, Jacob Sayono, and Yang Zhang. 2023. CubeSense++: Smart Environment Sensing with Interaction-Powered Corner Reflector Mechanisms. In *The 36th Annual ACM Symposium on User Interface Software and Technology (UIST '23), October 29-November 1, 2023, San Francisco, CA, USA.* ACM, New York, NY, USA, 12 pages. https://doi.org/10.1145/3586183.3606744

1 INTRODUCTION

Detection of occurrences or changes in events, such as human activities, object statuses, and environmental conditions, offers powerful insights about physical and social contexts, enabling computers in the environment to respond or anticipate to users' needs. Recognizing these events has long been of great interest to researchers. One straightforward approach is to equip sensors onto users or objects and examine unique signals resulted from activities of interest [4, 35, 36]. However, there exist challenges in massively deploying these sensors in the environment due to their reliance on batteries which often necessitate frequent maintenance. Other approaches include remote sensors that detect signals traveling through spaces, such as WiFi [40, 43, 57], sound [1], vibration [56], and light [17, 26] to infer event changes in the environment. However, these approaches usually rely on complicated learning-based inference techniques to leverage the implicit signal features, and are only capable of detecting a coarsely predefined set of activities, which limits their practicality due to the high diversity and granularity of activities in the environment.

All of the above factors hinder the large-scale implementation of sensors for smart environment sensing, prompting this research to explore alternative methods. Upon examining various activities and events in the environment, we observed that the occurrence of an activity usually involves physical movements of objects that users interact with. Prior research has been able to detect the presence of activities by the installation of tagging mechanisms that can be triggered by motions of objects. In a pioneering research, Mechanobeat [58] first introduced interaction-powered harmonic oscillation tagging mechanisms to highlight the use of objects' physical movement for activity recognition. However, only presence of activities can be detected while fine-grained information such as motion direction and speed is missing. This fine-grained information often constitutes an important contextual clue which is critical for smart devices to make better inferences about their users and surrounding environments.

We are inspired to expand the sensing capability by transforming movements of objects into encoded RF responses, from which fine-grained information about users and environments can be extracted using a millimeter wave radar from centralized sensor locations such as a smart light bulb on the ceiling or smart speakers on a countertop. Millimeter wave radar, typically used in automobile and security applications, has recently drawn the attention of researchers in HCI for its potential to be integrated into smart devices such as speakers, light bulbs, and thermostats to localize users and enable gestural input [23, 42]. Specifically, we explored using 3D printed corner reflector mechanisms to encode user interactions with everyday objects. These mechanisms do not rely on electronics or batteries, and can retrofit to a wide variety of everyday objects hitchhiking their inherent mechanical structures (e.g., gears, hinges, tracks). By decoding radar responses, fine-grained activity characteristics such as state, direction, rate, and usage can be inferred. We investigated effective corner reflector mechanism designs and developed the corresponding detection algorithm based on first-principle signal analysis. We demonstrated our system with 15 everyday objects (Figure 1) in indoor and outdoor environments.

2 RELATED WORK

2.1 Activity and Event Detection

Prior works detect occurrences of events that generate different types of signals, including visible light [33, 75], vibration [56, 78], RF broadcasts [5, 37, 62], acoustic signals [1, 36], electromagnetic interference (EMI) [8, 22, 79] and air pressure [46, 65]. In terms of sensor locations, researchers have developed wearable sensors to detect human activities [9, 31, 52]. Commercially available wearable sensors have seen success in health and fitness applications (e.g., smart ring [54]). Alternatively, sensors can be instrumented on objects of interest such as doors, microwaves, faucets to monitor their status [34, 77, 78].

These sensors are often powered by batteries, making their inevitable maintenance a significant cost of deploying them in the long run. To eliminate the reliance on batteries, researchers turned to develop self-powered sensors and systems that can harvest energy from environments [20, 75, 77] or from people [11, 68] to supply the power for sensing. Another approach to addressing power issue is to design sensors that contains no electronics and leverages material properties (i.e., type, geometry, motion pattern) for passive sensing [27, 30, 41, 58], with which our research shares the same scope.

2.2 RF Sensing in HCI

Radio Frequency (RF) sensing has long been sought after, with a majority of work focusing on the microwave range (e.g., WiFi, 2.4-5 GHz) [60, 74] and millimeter wave range (30-300 GHz) [42, 53, 62]. Operating at these special frequencies, RF signals enables high-fidelity sensing while preserving their innate advantages of being non-contact and not constrained by lighting conditions [76, 80].

RF sensing has been used in a wide array of applications including communications [44, 48], user identification and localization [55]. Other sensing modalities of prior works center around human activity recognition such as posture detection [32, 80], fall detection [63], vital signal [59, 70], eating behavior [66] and sleeping posture monitoring [71]. RF signals has also been used for sensing environmental facets such as sound [45], humidity [12], temperature[7], material [64, 72], and vibration [28].

The recent development of compact and solid-state millimeter wave radars such as Google Soli [42] opens up opportunities to enable interactive sensing such as hand gestures recognition [23], tangible interaction sensing [21], and interactive controls [25, 69]. Our system builds upon this growing interest but differs by shifting its focus from sensing human to sensing objects.

3 SENSING PRINCIPLE

3.1 FMCW Radar

Millimeter wave (mmWave) radar, has drawn attention from researchers in HCI due to its potential to enable a wide array of sensing modalities with a compact sensor form factor and limited privacy implications. At a frequency as high as 77 GHz, mmWave signals are less affected by interference from other sources such as Wi-Fi and Bluetooth signals, making it applicable for both indoor and outdoor environments. Radars can reveal rich information of targets including range and velocity, and those with beamforming capabilities can even sense multiple concurrent activities on targets scattered throughout the environment. Though radars are not as high-resolution as cameras, they can still yield sufficient information about targets such as shapes, deformation, posture changes for activity detection.

Radars that feature mmWave are usually modulated with Frequency Modulated Continuous Wave (FMCW) technology, which has been documented in prior work [23, 42, 76] and will not be detailed in this paper. In short, FMCW radar emits signals with linearly varying frequency, called chirps, and gets range and velocity of the target by measuring frequency and phase shift of the reflected signals. This chirp mechanism allows the detection of tiny displacement within a short duration (μs level), which is ideal for sensing moving objects. Besides, the power of received signals in a radar system with transmission power P_t, transmitter gain G_t, receiver gain G_r and wavelength λ, measured by Equation 1 [49], depends on the distance D between radar and the target, specifically its radar cross section (RCS) σ of the target and a loss factor L.

$$P_r = \frac{P_t G_t G_r \lambda^2 \sigma}{(4\pi)^3 D^4 L} \tag{1}$$

Though the reflectivity of a target (i.e., its RCS) is not the only factor that affect the magnitude of received signals, we found in practice that it is the dominant signal that explains the variance of received signals in the case of objects deployed in the environment. This is the main sensing principle we leverage in this paper – correlating the power of received signal with the RCS change of a target. Of note that the innate reflectivity changes of objects due to their movements in response to user interactions are modest, ambiguous, and heavily affected by variances in user motions, and thus we designed reflector mechanisms to encode these movements to facilitate their detection.

3.2 RF Reflector

RF reflectors are conventionally used to enhance RF reflections. They have been used for communication [44], localization [55], redirection [48], along with many novel use cases in research (e.g., CubeSense [69]). RF reflectors can be as simple as a flat metal sheet which appears as "a mirror" to incident waves. Leveraging the rapid development of wireless technologies such as Wi-Fi and radar, recent research has innovated reflectors with unique shapes, structures and materials that allow specific control of signal propagation, such as metasurfaces [2, 48], 3D-fabricated reflectors [67], frequency selective surface (FSS) reflectors [29].

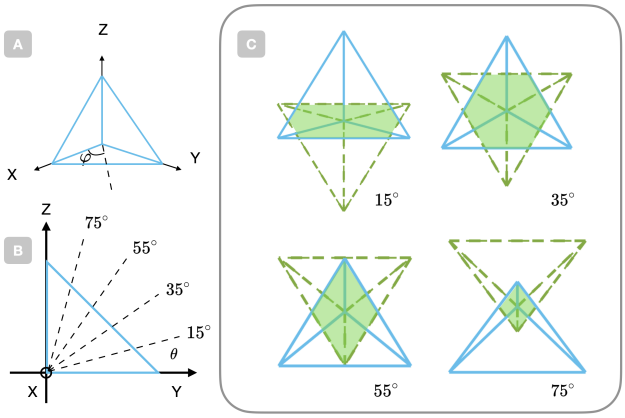

Figure 2: A: Front view of a triangular corner reflector. φ is the Azimuth angle. B: Side view of the reflector. θ is the Elevation angle. C: Effective aperture area (highlighted in green) with an incident angle of $\varphi = 45°$, $\theta = 15°, 35°, 55°, 75°$.

Retro-reflectors are a common type of RF reflectors that reflect RF waves back to their source. Van Atta array is a common retro-reflector that uses conductive antenna pairs with strategically designed lengths on planar surfaces to adjust the phase of incoming RF signals [55]. Corner reflectors, commonly made up of three mutually perpendicular plates, are often used in radar systems for detection [13, 73] and calibration [19]. Incident waves undergo multiple reflections within the "corner" and eventually reflected back to their sources. Note that this redirection of waves can happen only when incident waves land on certain areas of a corner reflector, denoted by effective aperture area A_{eff}. The effective aperture decides RCS, which describes the reflectivity of a corner reflector and is estimated by Equation 2, where λ is wavelength and R is the reflection coefficient derived from Fresnel equation [15, 16, 50].

$$\sigma = 4\pi R A_{eff}^2 / \lambda^2 \tag{2}$$

This equation shows three following factors that can change the magnitude of RCS, which we considered in the design of reflector mechanisms that encode user interactions into RCS changes. We selected corner reflectors to implement our reflector mechanisms for their following merits:

(1) They offer a relatively large RCS compared to their size, leading to a high Signal-to-Noise Ratio (SNR) and consequently improved detection capabilities.

(2) They provide wide-angle reflection, making them suitable for applications involving moving objects or unpredictable radar locations in the environment.

(3) Their RCS can be described mathematically, enabling the computational design of reflectors through first-principle approaches.

(4) Their simple structure and passive operation ensure durability, affordability, and ease of manufacture.

Factor 1: Material Interface materials can affect magnitude of reflected waves due to the difference in electrical properties, which can be measured in Equation 3 by the reflection coefficient:

$$R = \left| \frac{-\varepsilon_r \cos\theta_i + \sqrt{\varepsilon_r - \sin^2\theta_i}}{\varepsilon_r \cos\theta_i + \sqrt{\varepsilon_r - \sin^2\theta_i}} \right|^2 \quad (3)$$

where θ_i is the incident angle, and ε_r is the relative complex permittivity of a material given by $\varepsilon_r = \varepsilon' - j\frac{\sigma}{2\pi f \varepsilon_0}$ with the real part associated with degree of polarization of a material and the imaginary part the dielectric loss, σ is conductivity of the material, ε_0 is the vacuum permittivity, and f is the frequency of RF waves [16]. At radio frequencies, conductive materials such as metals exhibit a dominant imaginary part in their relative permittivity ε_r due to their high conductivity, which leads to higher reflectivity of radio waves [47]. Dielectric materials such as plastic, however, absorb radio waves due to lack of free electrons to radiate incoming signals as opposed to metals, and thus result in greater loss and smaller RCS [3]. In practice, we found that material is not an effective factor for tuning RCS because of the limited dynamic range resulted from common materials (e.g., plastic and metal).

Factor 2: Orientation A_{eff} is orientation-dependent and can be calculated as intersection between the open aperture and an inverted image aperture of corner reflector using geometric optics model [15]. Figure 2 shows an example of aperture area varying as the angle of the incident RF signal changes. To verify RCS changes with orientation, we ran a simulation with CST studio [10]. Specifically, we modeled a square corner reflector made of 5 cm perfect-electric-conductor (PEC) and swept both azimuth and elevation around 0-90°. Figure 3 A shows the simulated radiation pattern in 3D space. There are three side lobes besides the main lobe due to reflection on the three unit plates when the incident waves land perpendicular to them. This is aligned with the signal pattern we measured in the real world which we will discuss in Section 4.

Factor 3: Geometry Geometry includes the *shape* as well as the *size* of the unit plate on a corner reflector. Common shapes of a unit plate include triangular, circular and square. With the same shape, RCS varies with the edge length a, which decides the size of the unit plate and that of the overall corner reflector. Prior work has also proven $\sigma(a) \propto a^4$ at boresight [13–15]. To verify the correlation of RCS with a, we ran simulations for corner reflectors of 1-5 cm (at an 1 cm interval) edge length, and plotted RCS along the azimuth plane (with an Elevation angle of 35°). The result is shown in Figure 3 B, indicating that RCS increases with a for most incident Azimuth angles (i.e., 10 - 80°).

Furthermore, among these three factors (i.e., material, orientation, and geometry) on RCS of corner reflectors, we utilized *orientation* and *geometry* to induce RCS changes. Compared with these two factors, changes of *material* induce a narrower dynamic range of RCS and therefore was skipped in the implementation of our reflector mechanism. Our observation, as shown in Figure 3, unveils that rotations of a single corner reflector could induce RCS changes from a static radar's perspective. The rotation of one single corner induces periodic peaks of RF reflection which could reveal the status (i.e., on/off) and rate (i.e., speed and frequency) of activities. To encode richer information (e.g., direction), we concatenated multiple corner reflectors with different geometries along the periphery of a rotatory platform. The platform's rotation is driven by the movements of objects powered by user interactions through a linkage gear mechanism. Depending on the direction of rotation, the RF reflection will manifest as distinct time sequences, which can be exploited by a detection algorithm to decode directional information

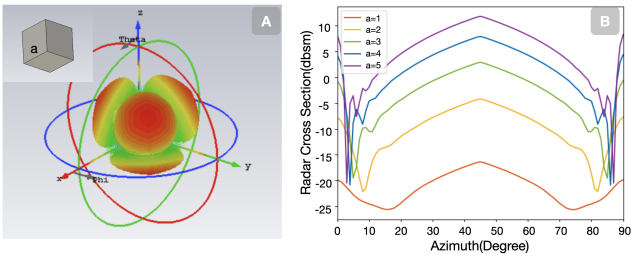

Figure 3: Simulation results. A: Radiation pattern of a square corner reflector (upper left: corner reflector model). B: RCS of corner reflector with different sizes ($\theta = 35°$).

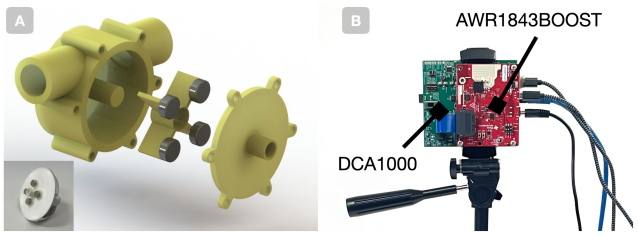

Figure 4: A: A pipe mechanism using magnetic coupling to enable an external rotation driven by the internal flow. The other set of magnets (shown at bottom left) is attached to the underside of the reflector. B: Radar sensor setup.

4 IMPLEMENTATION

4.1 Overview

Before detailing our system, we discuss some design considerations of reflector mechanisms that should be taken into account for achieving better sensing performance.

(1) The reflector mechanisms should generate signals with sufficient SNR to make it distinguishable in an environment, where stationary and dynamic objects (e.g., people and appliances in a home environment; moving cars and pedestrians in a city environment) constantly exist in the background. Strong and distinctive signals bolster the system's accuracy and reliability, ensuring its performance amid unpredictable background noise.

(2) The reflector mechanisms should encode different object status (e.g., on/off, direction, magnitude) with different signal characteristics (e.g., frequency, amplitude, phase). The difference between these signal patterns should be distinct and easy to be recognized by the radar receivers.

(3) The reflector mechanisms should be easy to fabricate, versatile to be instrumented on various host objects. They should be flexible and low-cost to deploy, and ideally have compact form factors for minimum intrusiveness.

Based on these considerations, we designed a series of electronic-free, 3D-printed reflector mechanisms for everyday objects, which can communicate with an millimeter wave radar wirelessly with rich information of their host objects. Specifically, to avoid interference of user movements, we encode speed of motions into frequency of signals, at a range much higher than human body movement (e.g., 1-3 steps/s while walking, running or jumping). Gear ratios were carefully selected in designing gear mechanisms that convert user interactions (i.e., object movements) into the rotation of our reflector mechanisms.

To detect direction of movements, we encode the direction of the reflector mechanism's rotation into the slope polarity of the envelope signal containing the reflection peaks induced by corner reflectors. By changing the geometry of the corner reflector facing toward the radar through the rotation of the reflector mechanism, it exhibits a gradual increase or decrease of RCS depending on the rotation direction (i.e., clockwise vs. counter-clockwise). We adopted a computational design approach to finalize the configurations of the reflector and proved its superiority against alternative designs.

4.2 Reflector Mechanism

4.2.1 Motion Transformation. We found three common types of movements on objects deployed in the environment: translational (i.e., sliding contact), rotational (i.e., hinged contact), and flow (i.e., fluid contact). These motions can be transformed by using mechanisms to achieve a desired rotational speed of the reflector mechanism.

To ensure optimal signal quality, the rotating speed (or frequency) of our reflector, denoted as $f_{reflector}$ in revolutions per second (or Hz), must have a high value that gives its motion signal a sufficient margin against signals induced by human body motion, denoted as f_{human}, and a maximum value that does not exceed $f_{radar}/2n$, where $f_{radar}/2$ is the Nyquist frequency of the maximum frame rate threshold of the radar f_{radar}, and n is the number of reflectors in the reflector mechanism. This relationship is captured by Equation 4. Additionally, the reflector must revolve at least one complete turn at every trial of the activity so that the signal can exhibit a gradual change in RCS.

$$f_{human} \ll f_{reflector} < f_{radar}/2n \tag{4}$$

Thus, for short-stroke motions such as hinged objects, which typically operate at a quarter revolution (for opening or closing), we design a mechanism with a 1:16 gear ratio to simultaneously satisfy both criteria. This allows the transformation of rotational motion to output a valid $f_{reflector}$ by multiplying the interaction speed by 16, ensuring a high enough frequency to be discriminated from human motion while allowing the reflector mechanism to revolve 4 times in a single operation. On the other hand, for long-stroke motions such as sliding objects or continuous stroke motions such as fluid flow, we design a mechanism with a 1:1 gear ratio, which we found sufficient to yield high-SNR signals.

4.2.2 Magnetic Coupling. The mechanism for the flow motion of liquid running inside pipes requires a special design (Figure 4 A). For example, the mechanism instrumented on an outdoor faucet has one end attached to the valve and the other end to the hose. We used magnetic coupling to facilitate movement between the water wheel driven by the internal water flow and the external fixture that rotates the reflector without having gaps that often cause leakage in our early iterations. The water wheel was 3D printed with PLA. We found that the mechanism could achieve high radial movement with minimal resistance, further reducing the risk of leaks and increasing durability over time.

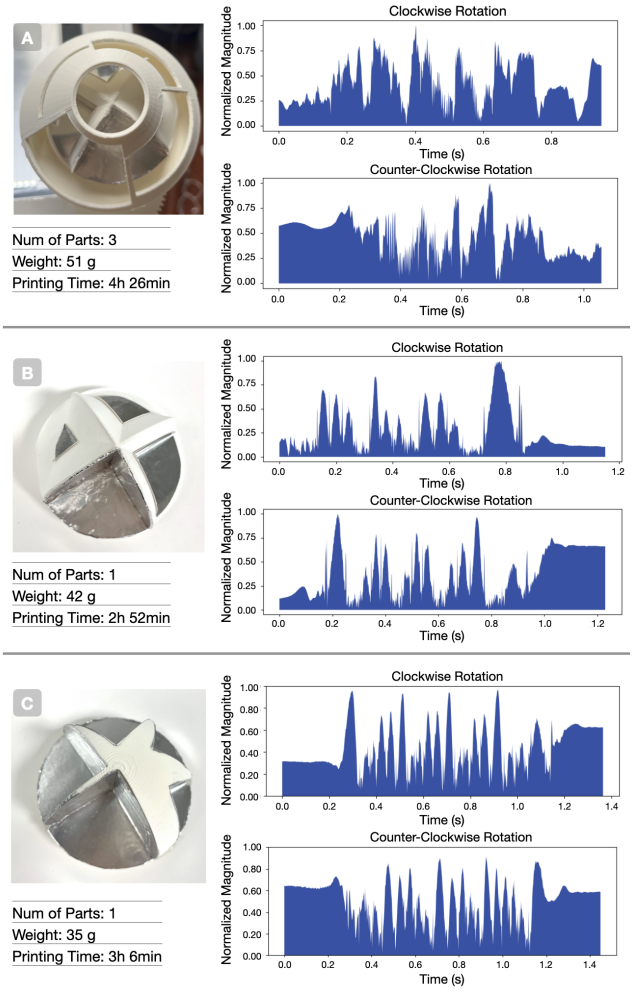

Figure 5: Geometry and signals of different reflectors. The weight and printing time are approximated based on the printing parameters used with the Ultimaker S5 3D Printer [51], including a layer height of 0.2 mm and 10 % infill. A: Reflector with cone-shaped shield. B: Hemisphere-shaped reflector with four parallel pockets. C: Hemisphere-shaped reflector with computationally designed pockets.

4.2.3 Reflector Geometry Design. First, we ensured the visibility of reflectors to radars at arbitrary deployment positions by having an array of corner reflectors on a hemisphere-shaped platform (i.e., a hemisphere-shaped reflector). Our reflector was designed with a hemisphere shape without sharp edges to be less intrusive to

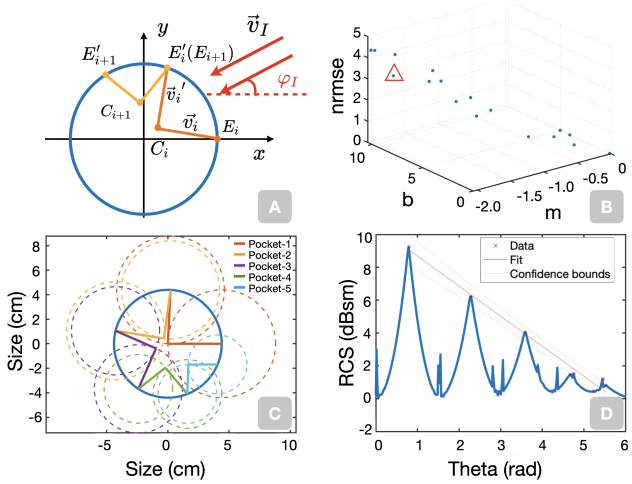

Figure 6: A: Top view of the hemisphere-shaped reflector, pocket arrangement and incident waves. B: Objective values of 18 solutions. C: Top view of reflector with radius=4.4, 4.0, 3.6, 2.8, 2.6 cm for pocket 1 - 5. D: Simulated RCS (i.e., H) of the reflector, peaks and the fitted model.

both users and environment, making it more practical in real-world applications. The corner reflectors on it ensure a wide range of workable incidence angles, allowing our reflector mechanisms to work with many radar locations (e.g., smart speakers, light bulbs).

Second, we select the approach to change reflectivity of the hemisphere-shaped reflector as it rotates. One straightforward approach is using a shield with various sizes of vents in front of a corner reflector to control the reflection of incoming signals. Specifically, we designed a cone-shaped shield with see-through vents that can rotate with gears, and a stationary corner reflector positioned inside the shield (Figure 5 A). We eventually abandoned this design for its delicate mechanical components, making it more challenging to set up (i.e., printing time, material consumption, and installation); and comparatively lower SNRs than the rest of the candidate designs.

We found it more feasible to leverage orientation and geometry factors discussed in Section 3, by concatenating multiple corner reflectors on a rotatory platform to get expected RF reflectivity pattern. In the following discussions, we use "pocket" to denote a single corner reflector on the hemisphere-shaped reflector. Our first prototype divided a hemisphere into four pockets with various sizes, and each with its edges parallel to those of its adjacent pocket (Figure 5 B). However, we found that it often yielded many side spikes of RF reflection, which we suspected were resulting from their unit plates when they were perpendicular to radar incident waves and from the margins between pockets. These side spikes pose challenges to our signal processing and information decoding algorithms and should be minimized, for which we decided to conduct another round of iteration.

We took a computational design approach for which we revised our design goal into: determining a concatenation of n pockets, with each pocket having an edge length of r_i, to have a monotonic RCS change across incident azimuth angles ranging from 0 to 360°.

Each pocket is described by $P_i = (C_i, E_i, E_i{}')$ with two edge vectors $\vec{v_i}$ and $\vec{v_i}'$. Edge vectors point from centers C_i to points on the hemisphere periphery E_i (Figure 6 A). Of note that $E_{i+1} = E_i{}'$. For each incident wave $\vec{v}_I(\varphi_I \in [0, 2\pi])$, we calculate RCS of the reflector across 0 - 360° by Equation 5, where $u(\cdot)$ is the unit step function neglecting pockets pointing away from the radar, $rcs(\cdot)$ is derived from simulation in Section 3 and $\rightarrow$ is a vector projection. Specifically, RCS of a corner reflector is symmetric along the boresight (i.e., Azimuth angle = 45°, Elevation angle = 35°), so we only consider the azimuth plane on the boresight. We further assumed that only those pockets, whose two edge vectors each form an angle between 0 and 90° with the incident vector, are capable of inducing a reflection back to the radar.

$$RCS(\vec{v}_I) = \sum_{i=1}^{n} u(\vec{v_i} \cdot \vec{v}_I) u(\vec{v_i}' \cdot \vec{v}_I) rcs(r_i, \vec{v}_I \rightarrow P_i) \tag{5}$$

Corner reflectors, even a small one, can induce strong reflection to the radar compared to environmental noise, resulting in a "peak" of radar response as it rotates. Pockets with different edge lengths yield different "peak" characteristics, which are what we leverage to encode information. This encoding mechanism is akin to amplitude modulation which has been widely used in communication. We define a new term to describe the hemisphere-shaped reflector that has a pocket array:

$$H = \underset{r_1, r_2, \ldots, r_n}{RCS(\vec{v}_I)} \tag{6}$$

We define peaks $(pk_1, pk_2, \ldots)$ induced when H rotates with certain constraints (i.e., the length of the peak array should be greater than 3) and fit them with a linear regression model using coefficients m, b and fitting error $rmse$. Then we solve the following constrained multi-objective optimization problem to find the optimal combination of pockets p_i,

$$\begin{aligned} \underset{r_1, r_2, \ldots, r_n}{\text{argmin}} \quad & m, -b, nrmse \\ \text{subject to} \quad & r_{min} \leq r_i \leq R, \\ & 0 \leq r_{i+1} - r_i, \\ & \sum_{i=1}^{n} \frac{2\pi r_i}{4} \leq 2\pi R. \end{aligned}$$

where $nrmse$ is the normalized fitting error, which we used to facilitate comparison between models. r_{min} is the radius of the smallest pocket bounded by environmental factors such as distance to the radar and ambient noise to ensure certain SNR (Equation 7). R is the radius of the hemisphere-shaped reflector. Of note that we assume that the hemisphere-shaped reflector rotates starting with the largest pocket facing the radar, and thus m needs to be as small as possible for yielding distinctive slope polarity, facilitating the direction detection. In the opposite rotation direction, m will guarantee to be the largest, assuring that one solution is optimal for both directions. We also reward a large b which is equivalent to a strong reflection when the largest pocket is facing the radar,

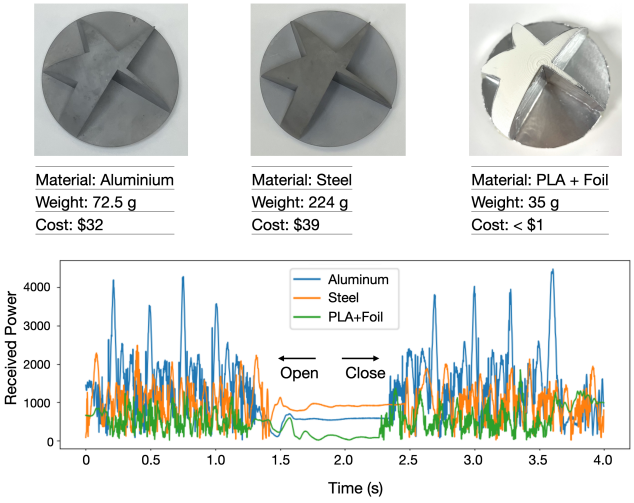

Figure 7: Reflectors made of Aluminium, Steel, and PLA; their fabrication details; and their signals collected from a mmWave radar positioned at 2.6 m away.

facilitating the detection of activity presence. This optimization problem is solved by a genetic search algorithm [6] in Matlab.

$$min\ r_i \propto \sigma_i \propto \frac{(SNR)P_{noise}(4\pi)^3 D^4 L}{P_t G_t G_r \lambda^2} \tag{7}$$

We empirically choose $n = 5, r_{min} = 1\ cm, R = 4.4\ cm$ for our reflector design, and a step of 0.2 cm for the searching space of r_i given our fabrication resolution. Figure 6 B shows objective function values at 18 different solutions. We selected one of the solutions by manually examining their simulated RCS patterns and picked the radius set of 4.4, 4.0, 3.6, 2.8, 2.6 cm for our design (Figure 6 C, D). This decision was based on design considerations such as RCS pattern including the number and magnitude of spikes, peak characteristics as well as the space efficiency of the pocket arrangement on the hemisphere. This computational design of reflectors strengthened their signal characteristic and facilitated their detection, for which we design a first-principle-based algorithm, as we will discuss in Section 4.4.

4.2.4 Reflector Material Selection. According to the discussion in Section 3.2, metals generally create stronger reflection than dielectric materials such as plastic, allowing more compact reflector designs that can be used in productization. We reached out to manufacturers and made reflectors out of aluminum alloy and steel with our computationally designed reflector geometry. Figure 7 shows results indicating that metal-printed reflectors induce strong reflection (2 - 4 times stronger than that of PLA + aluminum foil) and exhibit more distinctive signal patterns. However, metal fabrication was time- and cost-intensive due to its limited accessibility to the general public. This issue could become negligible once the fabrication of these reflectors transitions to a mass production scale. In this research, we followed a fabrication approach found effective in a prior work [69] to implement our reflector mechanisms, taking advantage of 3D printing as a rapid and cost-effective fabrication approach to yield complex and customized shapes. Specifically, we first 3D-printed reflector substrates out of PLA. To enhance reflectivity, we then attached a thin, conductive aluminum foil to the pockets of the hemisphere-shaped reflector. Our end result is low-cost, durable, and flexible to be deployed in various sizes.

4.3 Hardware

Our sensing system is based on TI's AWR1843 radar operating at 77-81 GHz. The sensor has three transmitters and four receivers with a 120° and 30° field of view in the Azimuth plane and Elevation plane respectively. We configured this radar to operate at a frame rate of 500 by sequentially emitting 1 chirp per transmitter per frame. We used this configuration to achieve a high frame rate of RCS sensing while being insensitive to velocity (i.e., speeds of object movement and reflector rotation) by not having multiple chirps within a frame. This is because our sensing principle is based on RCS changes rather than movements which often constitute noise (i.e., human motion) to our sensing. To ensure the separation of reflector mechanisms (~9 cm diameter) among objects, we used a chirp configuration of bandwidth = 1.8 GHz, chirp time = 60 μs, adc samples = 256, resulting in a maximum sensing range of 22 m and a range resolution of 9.7 cm. At this resolution, multiple objects could be easily separated so long as their reflector mechanisms are not sharing the same range-azimuth bin. Specifically, we measured that signals from a reflector are attenuated by -20dB in a bounding box (i.e., a potential location for another reflector) if the bounding box is placed 29 cm, 38 cm, 45 cm apart from the reflector at 1 m, 2 m and 3 m ranges. This measurement confirmed that our radar configuration is adequate for detecting multiple objects, since many household appliances (e.g., drawer, door) are spaced more than 1 m apart. The complex (I/Q) data samples are streamed by the DCA1000EVM data capture module to a laptop over an Ethernet cable for further processing.

4.4 Software

The raw ADC data, stored as a stream of 256x8 matrices, is processed with FFT to obtain range-azimuth profiles, allowing us to locate reflector mechanisms in the environment. We measure the average received power within a region of interest (ROI) over time and obtain a time sequence, to which a sliding window with 512 window length (WL) is applied to examine the signal characteristics and estimate the object status in real-time. Specifically, we used the following algorithm to determine the presence of an event, direction, speed, angle, and uses of target objects, where $Thred_{high}$ and $Thred_{low}$ are threshold values determined by host object and its environment, PW is minimum peak width used to eliminate spikes of noise. All the above parameters as well as the ranges and angles of the reflectors instrumented in the environment are obtained during system calibration. We developed Algorithm 1 for the detection of the presence and other rich information of events.

To demonstrate the effectiveness of our algorithm, we used data collected from one instrumented object (i.e., a CNC enclosure) as an example. Figure 8 shows the raw signals from a single trial of opening and closing, from which we can see that the event occurrence can be segmented by applying thresholds to the frequency spectrum. Figure 8 C and D show detailed characteristics of the time series, wherein the envelopes of peaks from an opening trial

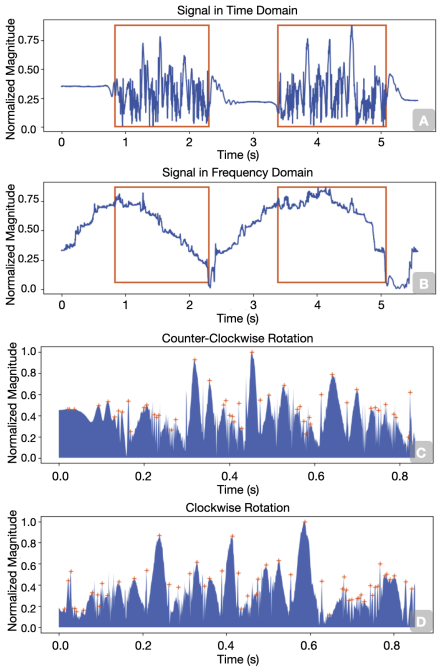

Figure 8: A: Signals of a single trial of opening and closing the CNC enclosure. B is obtained by applying FFT to signals within a window (size=512) that slides along the time axis and sums the high frequency components (> 50 Hz). C and D are signals from the two specific regions of A, with orange crosshairs representing the detected peaks.

feature a triangular wave pattern with a large peak followed by a decreasing ramp while a closing trial shows an increasing ramp followed by a sudden drop in signal magnitude. Furthermore, we collected data for different interaction scenarios including opening the CNC enclosure door at angles of 45°, 90°, 135° and 180° as well as at low, medium and high speed respectively. The results are shown in Figure 9, indicating the feasibility of sensing these fine-grained information about activities with our encoding mechanism and detection algorithm.

5 EVALUATION

We deployed 14 mechanisms in two indoor environments (i.e., maker space and office) and one outdoor environment (i.e., house

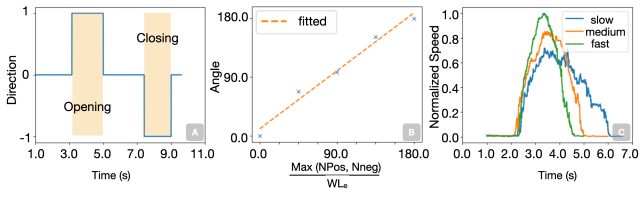

Figure 9: Fine-grained information about activities including direction (A), angle (B), and speed (C) can be detected.

Algorithm 1 Event detection algorithm

Input: signal sequence $w_1, w_2, ..., w_n$
Output: $Presence, Speed, Angle, Direction$

while w_i received **do**
  $f_{w_i} = FFT(w_i)$, apply a low pass filter on f_{w_i}
  sum high frequency bins of f_{w_i} to obtain f_{hf}
  if $f_{hf} \in (Thred_{high}, Thred_{low})$ **then**
    presence = true -> **presence**
  end if
  $peaks = findPeaks(w_i, PW)$
  calculate derivative of $peaks$, count number of positive derivative $NPos$ and negative derivative $NNeg$
end while
obtain w_e from all w_i with $Presence = true$
while w_e exists, window size WL_e **do**
  $peaks_e = findPeaks(w_e, PW)$
  calculate derivative $peaks_{diff}$
  get $idx = max(abs(peaks_{diff}))$
  direction $\propto$ polarity of $peaks_{diff}(idx)$ -> **direction**
  angle $\propto \frac{\max(NPos, NNeg)}{WL_e}$ -> **angle**
  speed $\propto f_{hf}$ -> **speed**
end while

backyard), as shown in Figure 10. Details of these mechanisms can be found in Figure 1. Of note that we omitted the anemometer for the difficulty of inducing its ground-truth signals in the study. At each location, the radar sensor was affixed at a certain location and went through a calibration process prior to the testing. This process included adjusting orientation, selecting a region of interest, and setting thresholds. Two experimenters conducted three rounds of testing for each object at each location. Specifically, one round of testing started with a 10-minute data collection during which objects were idle and experimenters performed daily activities such as working, talking, eating, walking, and exercising. Then, an experimenter performed 10 trials of operation on one object (i.e., one trial includes one complete opening and one closing operation) with approximately 2 seconds interval, until all objects were tested. The environments were occupied and exposed to users and elements expected to be seen in everyday settings (e.g., users walking in the maker space, windy weather in the backyard).

An example of signals from one round of testing (i.e., 10-minute data and 20 trials) for the storage container is shown in Figure 11. We found that signals resulting from reflector mechanisms (i.e., the thick oscillations in Figure 11 B and C) were much more distinctive than idle signals (i.e., signals in between oscillations). We also observed that activities involving RF reflective materials, such as opening or closing a laptop (spikes in Figure 11 A), had a higher chance of triggering false positive detection. This observation was common across all objects we tested in this study and validated the effectiveness of our reflector design.

Our dataset consisted of 840 trials of operation, and the results showed a low false positive rate (only 5 times out of all the 10-minute idle data collection from the 14 mechanisms, counting 7 hours in total) and a true positive rate of 98.25% for use detection. On average, direction detection accuracy was 80.2%. The table at

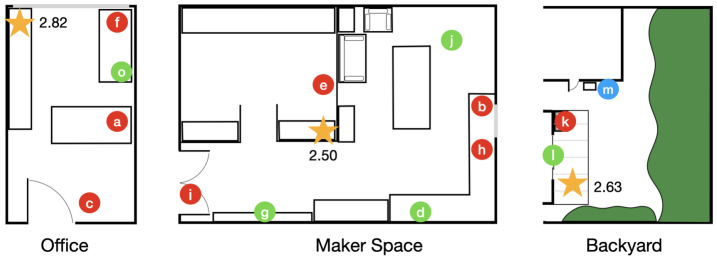

Location	Object	Distance to sensor (m)	Event Existence Detection		Direction Detection	
			Quiet Environment	Occupied Environment	Quiet Environment	Occupied Environment
Office	Table Lamp (f)	2.52	0.90	0.97	0.72	0.72
	Microwave (a)	3.02	1.00	1.00	0.83	0.78
	Trash Bin (c)	3.97	0.98	0.98	0.83	0.80
	Standing Desk (o)	2.85	0.97	0.97	0.80	0.82
Maker Space	CNC Machine (b)	3.22	0.98	0.98	0.82	0.83
	Backdrop (d)	3.07	0.93	0.97	0.70	0.75
	Fridge (e)	2.72	0.98	0.93	0.75	0.80
	Storage Container (g)	3.00	1.00	1.00	0.87	0.83
	3D Printer (h)	4.65	1.00	1.00	0.80	0.75
	Hinged Door (i)	5.20	0.98	0.97	0.68	0.72
	Treadmill (j)	3.80	1.00	1.00	–	
Backyard	Grill (k)	2.50	1.00	1.00	0.82	0.85
	Sliding Door (l)	1.94	1.00	1.00	0.82	0.85
	Faucet (m)	5.52	0.97	0.97	–	

Figure 10: Deployment details. Left: Floor plans of the three locations in the evaluation. Colored dots are objects instrumented with mechanisms as shown in Figure 1. The orange stars denote the radar sensor with the number indicating its height to the ground (in meters). Right: Detection accuracies. Note that the treadmill and faucet are unidirectional objects and were excluded from the evaluation of the direction detection.

the right side of Figure 10 shows the detection accuracies for each object. We found a minimum impact from the variations in environments and object locations on the detection of object use. A more significant impact was found on the detection of direction. As the distance between objects and the radar sensors increased, the direction detection accuracy decreased, for the lower SNR due to the larger path loss of radar signals during the transmission.

6 DISCUSSION

One obvious limitation is the limited sensing capability on objects out of radar's line of sight. The penetration capability of RF waves decreases with their wavelength in the GHz frequency bands assuming a constant power. However, shorter waves enable sensing with higher spatial resolutions that allow better differentiation between

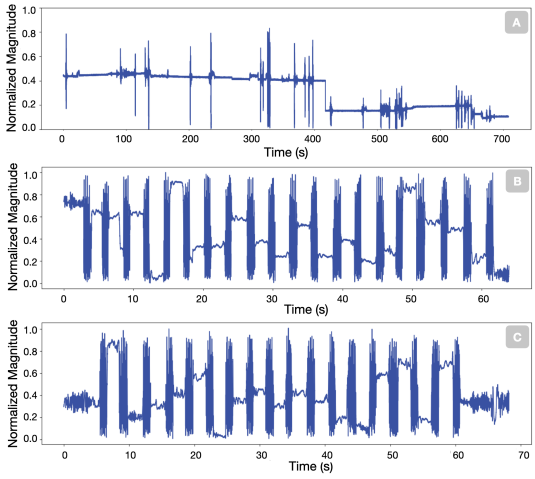

Figure 11: A round of testing for the storage container. Ten minutes of data collected when no objects were in use in an occupied environment (A). One minute of 10 trials of operation in a quiet environment (B) and in a busy environment where people were walking around (C).

multiple objects in the environment as well as smaller reflector form factors. To mitigate this limitation, one possible solution is to leverage reflections of RF waves on everyday surfaces. This solution has shown promise in prior works demonstrating Non-line-of-sight (NLOS) radar sensing techniques [18, 24, 61].

Currently, reflectors are registered to locations (i.e., unique combinations of Range, Azimuth, and Elevation) of their host objects, thus necessitating a manual calibration process. However, this calibration is only required at the installation or when object location changes, which is often infrequent for many objects (e.g., facets, doors, windows). The effort required for calibration is comparable to setting up new IoT devices. Nonetheless, we recognize this as a limitation of our current approach. Sensing movable objects is unachievable through this location-based identification. Looking ahead, hybrid sensing approaches (e.g., with RFID) and advanced signal processing could potentially facilitate the identification of objects and thus eliminate the need for calibration.

Another challenge is the design of gear mechanisms that retrofit existing environments. Particularly for hinged objects, the axis of rotation is difficult to locate. We expect sensor-aided approaches using vision or IMU sensors on mobile devices to be possible, as shown in prior work [38, 39]. Additionally, the gear mechanisms are bulky in our current design, however, smaller gearboxes exist and could be achieved with superior fabrication methods (e.g., metal printing). A long-term solution to eliminate a user's installation effort and to minimize the reflector form factor is to integrate the reflector mechanism into the manufacture of everyday objects, or to be provided as accessories by the manufacturers as an optional enhancement (akin to the furniture wall straps).

Though we did not demonstrate concurrent activity sensing, we noted that activities that are sufficiently separated should be able to be independently detected due to the minimal interference caused by overlapping of reflection on the range-azimuth map. Nonetheless, further research is necessary to extensively explore its feasibility. Future work could utilize advanced beam-forming approaches to distinguish signals from various sources in complex environments that involve multi-path interference, as well as overcome security

challenges including spoofing and MITM attacks, both of which are limitations of our sensing approach.

7 CONCLUSION

We introduced a new method of utilizing mmWave radar for detecting activities in user environments. Our approach enables various sensing modes that take advantage of low-cost reflector mechanisms which are entirely passive to encode activities to characteristic RF reflections. With a careful computationally generated design, these reflectors can facilitate a wide range of smart environment applications that currently rely on more expensive and high-maintenance infrastructure. In addition to detecting the presence of activities, our approach also detects the direction and speed/rate of activities yielding richer contextual information. The study conducted at three different locations demonstrates the robustness of our approach with extremely low false positive rates across distances and angles. We envision our approach to be incorporated into future IoT devices such as smart light bulbs, speakers, thermostats, and service robots, to enhance their capacity to infer user context and thus improve their capability to serve.

ACKNOWLEDGMENTS

We thank Chris Harrison for his help with brainstorming. This research was supported by the National Science Foundation (IIS-2228982). We also thank Keysight for their generous donation.

REFERENCES

[1] Rebecca Adaimi, Howard Yong, and Edison Thomaz. 2021. Ok Google, What Am I Doing? Acoustic Activity Recognition Bounded by Conversational Assistant Interactions. *Proc. ACM Interact. Mob. Wearable Ubiquitous Technol.* 5, 1, Article 2 (mar 2021), 24 pages. https://doi.org/10.1145/3448090

[2] VS Asadchy, Ana Díaz-Rubio, SN Tcvetkova, D-H Kwon, Amr Elsakka, Mohamed Albooyeh, and SA Tretyakov. 2017. Flat engineered multichannel reflectors. *Physical Review X* 7, 3 (2017), 031046.

[3] Christian Buchberger, Florian Pfeiffer, and Erwin Biebl. 2019. Dielectric corner reflectors for mmWave applications. *Advances in Radio Science* 17 (2019), 197–203.

[4] Michael Buettner, Richa Prasad, Matthai Philipose, and David Wetherall. 2009. Recognizing Daily Activities with RFID-Based Sensors. In *Proceedings of the 11th International Conference on Ubiquitous Computing* (Orlando, Florida, USA) *(UbiComp '09)*. Association for Computing Machinery, New York, NY, USA, 51–60. https://doi.org/10.1145/1620545.1620553

[5] Michael Buettner, Richa Prasad, Matthai Philipose, and David Wetherall. 2009. Recognizing Daily Activities with RFID-Based Sensors. In *Proceedings of the 11th International Conference on Ubiquitous Computing* (Orlando, Florida, USA) *(UbiComp '09)*. Association for Computing Machinery, New York, NY, USA, 51–60. https://doi.org/10.1145/1620545.1620553

[6] Yair Censor. 1977. Pareto optimality in multiobjective problems. *Applied Mathematics and Optimization* 4, 1 (1977), 41–59.

[7] Baicheng Chen, Huining Li, Zhengxiong Li, Xingyu Chen, Chenhan Xu, and Wenyao Xu. 2020. ThermoWave: a new paradigm of wireless passive temperature monitoring via mmWave sensing. In *Proceedings of the 26th Annual International Conference on Mobile Computing and Networking*. 1–14.

[8] Ke-Yu Chen, Sidhant Gupta, Eric C. Larson, and Shwetak Patel. 2015. DOSE: Detecting user-driven operating states of electronic devices from a single sensing point. In *2015 IEEE International Conference on Pervasive Computing and Communications (PerCom)*. 46–54. https://doi.org/10.1109/PERCOM.2015.7146508

[9] Gabe Cohn, Sidhant Gupta, Tien-Jui Lee, Dan Morris, Joshua R Smith, Matthew S Reynolds, Desney S Tan, and Shwetak N Patel. 2012. An ultra-low-power human body motion sensor using static electric field sensing. In *Proceedings of the 2012 ACM conference on ubiquitous computing*. 99–102.

[10] Software Information. CST. CST n.d.. CST STUDIO SUITE. 2023. https://www.3ds.com/products-services/simulia/products/cst-studio-suit Last accessed 20 March 2023.

[11] Alexander Curtiss, Blaine Rothrock, Abu Bakar, Nivedita Arora, Jason Huang, Zachary Englhardt, Aaron-Patrick Empedrado, Chixiang Wang, Saad Ahmed, Yang Zhang, et al. 2021. FaceBit: Smart face masks platform. *Proceedings of the ACM on Interactive, Mobile, Wearable and Ubiquitous Technologies* 5, 4 (2021), 1–44.

[12] Qinglang Dai, Yongzhi Huang, Lu Wang, Rukhsana Ruby, and Kaishun Wu. 2018. mm-humidity: Fine-grained humidity sensing with millimeter wave signals. In *2018 IEEE 24th International Conference on Parallel and Distributed Systems (ICPADS)*. IEEE, 204–211.

[13] Armin Walter Doerry. 2014. *Reflectors for SAR performance testing*. Technical Report. Sandia National Lab.(SNL-NM), Albuquerque, NM (United States).

[14] Armin W Doerry and Billy C Brock. 2009. Radar cross section of triangular trihedral reflector with extended bottom plate. *Sandia Report, Sandia National Laboratory* (2009).

[15] HD Eckhardt. 1971. Simple model of corner reflector phenomena. *Applied Optics* 10, 7 (1971), 1559–1566.

[16] Fresnel equation. 2023. https://en.wikipedia.org/wiki/Fresnel_equations Last accessed 20 March 2023.

[17] Nathaniel Faulkner, Fakhrul Alam, Mathew Legg, and Serge Demidenko. 2019. Watchers on the wall: Passive visible light-based positioning and tracking with embedded light-sensors on the wall. *IEEE Transactions on Instrumentation and Measurement* 69, 5 (2019), 2522–2532.

[18] Chao Feng, Xinyi Li, Yangfan Zhang, Xiaojing Wang, Liqiong Chang, Fuwei Wang, Xinyu Zhang, and Xiaojiang Chen. 2021. RFlens: metasurface-enabled beamforming for IoT communication and sensing. In *Proceedings of the 27th Annual International Conference on Mobile Computing and Networking*. 587–600.

[19] A Laurence Gray, Paris W Vachon, Charles E Livingstone, and Tom I Lukowski. 1990. Synthetic aperture radar calibration using reference reflectors. *IEEE Transactions on Geoscience and Remote Sensing* 28, 3 (1990), 374–383.

[20] Manoj Gulati, Farshid Salemi Parizi, Eric Whitmire, Sidhant Gupta, Shobha Sundar Ram, Amarjeet Singh, and Shwetak N. Patel. 2018. CapHarvester: A Stick-on Capacitive Energy Harvester Using Stray Electric Field from AC Power Lines. *Proc. ACM Interact. Mob. Wearable Ubiquitous Technol.* 2, 3, Article 110 (Sept. 2018), 20 pages. https://doi.org/10.1145/3264920

[21] Tamil Selvan Gunasekaran, Ryo Hajika, Yun Suen Pai, Eiji Hayashi, and Mark Billinghurst. 2022. RaITIn: Radar-Based Identification for Tangible Interactions *(CHI EA '22)*. Association for Computing Machinery, New York, NY, USA, Article 445, 7 pages. https://doi.org/10.1145/3491101.3519808

[22] Sidhant Gupta, Matthew S. Reynolds, and Shwetak N. Patel. 2010. ElectriSense: Single-Point Sensing Using EMI for Electrical Event Detection and Classification in the Home. In *Proceedings of the 12th ACM International Conference on Ubiquitous Computing* (Copenhagen, Denmark) *(UbiComp '10)*. Association for Computing Machinery, New York, NY, USA, 139–148. https://doi.org/10.1145/1864349.1864375

[23] Eiji Hayashi, Jaime Lien, Nicholas Gillian, Leonardo Giusti, Dave Weber, Jin Yamanaka, Lauren Bedal, and Ivan Poupyrev. 2021. RadarNet: Efficient Gesture Recognition Technique Utilizing a Miniature Radar Sensor. In *Proceedings of the 2021 CHI Conference on Human Factors in Computing Systems* (Yokohama, Japan) *(CHI '21)*. Association for Computing Machinery, New York, NY, USA, Article 5, 14 pages. https://doi.org/10.1145/3411764.3445367

[24] Jianghaomiao He, Shota Terashima, Hideyuki Yamada, and Shouhei Kidera. 2021. Diffraction signal-based human recognition in non-line-of-sight (NLOS) situation for millimeter wave radar. *IEEE Journal of Selected Topics in Applied Earth Observations and Remote Sensing* 14 (2021), 4370–4380.

[25] Yuqian Hu, Beibei Wang, Chenshu Wu, and KJ Ray Liu. 2021. mmKey: Universal Virtual Keyboard Using A Single Millimeter-Wave Radio. *IEEE Internet of Things Journal* 9, 1 (2021), 510–524.

[26] Mohamed Ibrahim, Viet Nguyen, Siddharth Rupavatharam, Minitha Jawahar, Marco Gruteser, and Richard Howard. 2016. Visible Light Based Activity Sensing Using Ceiling Photosensors. In *Proceedings of the 3rd Workshop on Visible Light Communication Systems* (New York City, New York) *(VLCS '16)*. Association for Computing Machinery, New York, NY, USA, 43–48. https://doi.org/10.1145/2981548.2981554

[27] Vikram Iyer, Justin Chan, and Shyamnath Gollakota. 2017. 3D Printing Wireless Connected Objects. *ACM Transactions on Graphics (TOG)*.

[28] Chengkun Jiang, Junchen Guo, Yuan He, Meng Jin, Shuai Li, and Yunhao Liu. 2020. mmVib: micrometer-level vibration measurement with mmwave radar. In *Proceedings of the 26th Annual International Conference on Mobile Computing and Networking*. 1–13.

[29] Alejandro Jiménez-Sáez, Martin Schüßler, Mohammed El-Absi, Ali Alhaj Abbas, Klaus Solbach, Thomas Kaiser, and Rolf Jakoby. 2020. Frequency selective surface coded retroreflectors for chipless indoor localization tag landmarks. *IEEE Antennas and Wireless Propagation Letters* 19, 5 (2020), 726–730.

[30] Haojian Jin, Jingxian Wang, Zhijian Yang, Swarun Kumar, and Jason Hong. 2018. Wish: Towards a wireless shape-aware world using passive rfids. In *Proceedings of the 16th Annual International Conference on Mobile Systems, Applications, and Services*. 428–441.

[31] Haruka Kamachi, Tahera Hossain, Fuyuka Tokuyama, Anna Yokokubo, and Guillaume Lopez. 2021. Prediction of Eating Activity Using Smartwatch. In *Adjunct Proceedings of the 2021 ACM International Joint Conference on Pervasive and Ubiquitous Computing and Proceedings of the 2021 ACM International Symposium on Wearable Computers* (Virtual, USA) *(UbiComp '21)*. Association for Computing Machinery, New York, NY, USA, 304–309. https://doi.org/10.1145/3460418.3479348

[32] Hao Kong, Xiangyu Xu, Jiadi Yu, Qilin Chen, Chenguang Ma, Yingying Chen, Yi-Chao Chen, and Linghe Kong. 2022. m3track: mmwave-based multi-user 3d posture tracking. In *Proceedings of the 20th Annual International Conference on Mobile Systems, Applications and Services*. 491–503.

[33] Daniel Konings, Nathaniel Faulkner, Fakhrul Alam, Edmund M-K Lai, and Serge Demidenko. 2019. FieldLight: Device-free indoor human localization using passive visible light positioning and artificial potential fields. *IEEE Sensors Journal* 20, 2 (2019), 1054–1066.

[34] Stacey Kuznetsov and Eric Paulos. 2010. UpStream: motivating water conservation with low-cost water flow sensing and persuasive displays. In *Proceedings of the SIGCHI Conference on Human Factors in Computing Systems*. 1851–1860.

[35] Gierad Laput and Chris Harrison. 2019. Sensing Fine-Grained Hand Activity with Smartwatches. In *Proceedings of the 2019 CHI Conference on Human Factors in Computing Systems* (Glasgow, Scotland Uk) *(CHI '19)*. Association for Computing Machinery, New York, NY, USA, 1–13. https://doi.org/10.1145/3290605.3300568

[36] Gierad Laput, Robert Xiao, and Chris Harrison. 2016. ViBand: High-Fidelity Bio-Acoustic Sensing Using Commodity Smartwatch Accelerometers. In *Proceedings of the 29th Annual Symposium on User Interface Software and Technology* (Tokyo, Japan) *(UIST '16)*. Association for Computing Machinery, New York, NY, USA, 321–333. https://doi.org/10.1145/2984511.2984582

[37] Hanchuan Li, Can Ye, and Alanson P. Sample. 2015. IDSense: A Human Object Interaction Detection System Based on Passive UHF RFID. In *Proceedings of the 33rd Annual ACM Conference on Human Factors in Computing Systems* (Seoul, Republic of Korea) *(CHI '15)*. Association for Computing Machinery, New York, NY, USA, 2555–2564. https://doi.org/10.1145/2702123.2702178

[38] Jiahao Li, Jeeeun Kim, and Xiang'Anthony' Chen. 2019. Robiot: A design tool for actuating everyday objects with automatically generated 3D printable mechanisms. In *Proceedings of the 32nd Annual ACM Symposium on User Interface Software and Technology*. 673–685.

[39] Jiahao Li, Alexis Samoylov, Jeeeun Kim, and Xiang'Anthony' Chen. 2022. Roman: Making Everyday Objects Robotically Manipulable with 3D-Printable Add-on Mechanisms. In *Proceedings of the 2022 CHI Conference on Human Factors in Computing Systems*. 1–17.

[40] Shengjie Li, Xiang Li, Qin Lv, Guiyu Tian, and Daqing Zhang. 2018. WiFit: Ubiquitous bodyweight exercise monitoring with commodity wi-fi devices. In *2018 IEEE SmartWorld, Ubiquitous Intelligence & Computing, Advanced & Trusted Computing, Scalable Computing & Communications, Cloud & Big Data Computing, Internet of People and Smart City Innovation (SmartWorld/SCALCOM/UIC/ATC/CBDCom/IOP/SCI)*. IEEE, 530–537.

[41] Zhengxiong Li, Baicheng Chen, Zhuolin Yang, Huining Li, Chenhan Xu, Xingyu Chen, Kun Wang, and Wenyao Xu. 2019. Ferrotag: A paper-based mmwave-scannable tagging infrastructure. In *Proceedings of the 17th Conference on Embedded Networked Sensor Systems*. 324–337.

[42] Jaime Lien, Nicholas Gillian, M. Emre Karagozler, Patrick Amihood, Carsten Schwesig, Erik Olson, Hakim Raja, and Ivan Poupyrev. 2016. Soli: Ubiquitous Gesture Sensing with Millimeter Wave Radar. *ACM Trans. Graph.* 35, 4, Article 142 (jul 2016), 19 pages. https://doi.org/10.1145/2897824.2925953

[43] Francesca Meneghello, Domenico Garlisi, Nicolò Dal Fabbro, Ilenia Tinnirello, and Michele Rossi. 2022. SHARP: Environment and Person Independent Activity Recognition with Commodity IEEE 802.11 Access Points. *IEEE Transactions on Mobile Computing* (2022).

[44] John Nolan, Kun Qian, and Xinyu Zhang. 2021. RoS: passive smart surface for roadside-to-vehicle communication. In *Proceedings of the 2021 ACM SIGCOMM 2021 Conference*. 165–178.

[45] Muhammed Zahid Ozturk, Chenshu Wu, Beibei Wang, and KJ Liu. 2021. Radiomic: Sound sensing via mmwave signals. *arXiv preprint arXiv:2108.03164* (2021).

[46] Shwetak N Patel, Matthew S Reynolds, and Gregory D Abowd. 2008. Detecting human movement by differential air pressure sensing in HVAC system ductwork: An exploration in infrastructure mediated sensing. In *Pervasive Computing: 6th International Conference, Pervasive 2008 Sydney, Australia, May 19-22, 2008 Proceedings 6*. Springer, 1–18.

[47] Relative permittivity. 2023. https://en.wikipedia.org/wiki/Relative_permittivity Last accessed 27 July 2023.

[48] Kun Qian, Lulu Yao, Xinyu Zhang, and Tse Nga Ng. 2022. MilliMirror: 3D Printed Reflecting Surface for Millimeter-Wave Coverage Expansion *(MobiCom '22)*. Association for Computing Machinery, New York, NY, USA, 15–28. https://doi.org/10.1145/3495243.3517024

[49] Radar quation. 2023. https://www.radartutorial.eu/01.basics/The%20Radar%20Range%20Equation.en.html Last accessed 20 March 2023.

[50] Corner reflector. 2023. https://www.radartutorial.eu/17.bauteile/bt47.en.html Last accessed 24 July 2023.

[51] Ultimaker S5. 2023. https://ultimaker.com/3d-printers/s-series/ultimaker-s5/ Last accessed 20 July 2023.

[52] Farhad Shahmohammadi, Anahita Hosseini, Christine E King, and Majid Sarrafzadeh. 2017. Smartwatch based activity recognition using active learning. In *2017 IEEE/ACM International Conference on Connected Health: Applications, Systems and Engineering Technologies (CHASE)*. IEEE, 321–329.

[53] Akash Deep Singh, Sandeep Singh Sandha, Luis Garcia, and Mani Srivastava. 2019. RadHAR: Human Activity Recognition from Point Clouds Generated through a Millimeter-Wave Radar. In *Proceedings of the 3rd ACM Workshop on Millimeter-Wave Networks and Sensing Systems* (Los Cabos, Mexico) *(mmNets'19)*. Association for Computing Machinery, New York, NY, USA, 51–56. https://doi.org/10.1145/3349624.3356768

[54] Oura smart ring. 2023. https://ouraring.com/ Last accessed 20 March 2023.

[55] Elahe Soltanaghaei, Akarsh Prabhakara, Artur Balanuta, Matthew Anderson, Jan M. Rabaey, Swarun Kumar, and Anthony Rowe. 2021. Millimetro: MmWave Retro-Reflective Tags for Accurate, Long Range Localization. In *Proceedings of the 27th Annual International Conference on Mobile Computing and Networking* (New Orleans, Louisiana) *(MobiCom '21)*. Association for Computing Machinery, New York, NY, USA, 69–82. https://doi.org/10.1145/3447993.3448627

[56] Wei Sun, Tuochao Chen, Jiayi Zheng, Zhenyu Lei, Lucy Wang, Benjamin Steeper, Peng He, Matthew Dressa, Feng Tian, and Cheng Zhang. 2020. VibroSense: Recognizing Home Activities by Deep Learning Subtle Vibrations on an Interior Surface of a House from a Single Point Using Laser Doppler Vibrometry. *Proc. ACM Interact. Mob. Wearable Ubiquitous Technol.* 4, 3, Article 96 (sep 2020), 28 pages. https://doi.org/10.1145/3411828

[57] Sheng Tan, Linghan Zhang, Zi Wang, and Jie Yang. 2019. MultiTrack: Multi-user tracking and activity recognition using commodity WiFi. In *Proceedings of the 2019 CHI Conference on Human Factors in Computing Systems*. 1–12.

[58] Md Farhan Tasnim Oshim, Julian Killingback, Dave Follette, Huaishu Peng, and Tauhidur Rahman. 2020. MechanoBeat: Monitoring Interactions with Everyday Objects using 3D Printed Harmonic Oscillators and Ultra-Wideband Radar. In *Proceedings of the 33rd Annual ACM Symposium on User Interface Software and Technology*. 430–444.

[59] Fengyu Wang, Xiaolu Zeng, Chenshu Wu, Beibei Wang, and KJ Ray Liu. 2021. mmHRV: Contactless heart rate variability monitoring using millimeter-wave radio. *IEEE Internet of Things Journal* 8, 22 (2021), 16623–16636.

[60] Hao Wang, Daqing Zhang, Yasha Wang, Junyi Ma, Yuxiang Wang, and Shengjie Li. 2016. RT-Fall: A real-time and contactless fall detection system with commodity WiFi devices. *IEEE Transactions on Mobile Computing* 16, 2 (2016), 511–526.

[61] Ruiyu Wang, Paulo Valente Klaine, Oluwakayode Onireti, Yao Sun, Muhammad Ali Imran, and Lei Zhang. 2021. Deep learning enabled beam tracking for non-line of sight millimeter wave communications. *IEEE Open Journal of the Communications Society* 2 (2021), 1710–1720.

[62] Yuheng Wang, Haipeng Liu, Kening Cui, Anfu Zhou, Wensheng Li, and Huadong Ma. 2021. m-activity: Accurate and real-time human activity recognition via millimeter wave radar. In *ICASSP 2021-2021 IEEE International Conference on Acoustics, Speech and Signal Processing (ICASSP)*. IEEE, 8298–8302.

[63] Yuxi Wang, Kaishun Wu, and Lionel M Ni. 2016. Wifall: Device-free fall detection by wireless networks. *IEEE Transactions on Mobile Computing* 16, 2 (2016), 581–594.

[64] Chenshu Wu, Feng Zhang, Beibei Wang, and KJ Ray Liu. 2020. msense: Towards mobile material sensing with a single millimeter-wave radio. *Proceedings of the ACM on Interactive, Mobile, Wearable and Ubiquitous Technologies* 4, 3 (2020), 1–20.

[65] Muchen Wu, Parth H. Pathak, and Prasant Mohapatra. 2015. Monitoring Building Door Events Using Barometer Sensor in Smartphones. In *Proceedings of the 2015 ACM International Joint Conference on Pervasive and Ubiquitous Computing* (Osaka, Japan) *(UbiComp '15)*. Association for Computing Machinery, New York, NY, USA, 319–323. https://doi.org/10.1145/2750858.2804257

[66] Yucheng Xie, Ruizhe Jiang, Xiaonan Guo, Yan Wang, Jerry Cheng, and Yingying Chen. 2022. mmEat: Millimeter wave-enabled environment-invariant eating behavior monitoring. *Smart Health* 23 (2022), 100236. https://doi.org/10.1016/j.smhl.2021.100236

[67] Xi Xiong, Justin Chan, Ethan Yu, Nisha Kumari, Ardalan Amiri Sani, Changxi Zheng, and Xia Zhou. 2017. Customizing Indoor Wireless Coverage via 3D-Fabricated Reflectors. In *Proceedings of the 4th ACM International Conference on Systems for Energy-Efficient Built Environments* (Delft, Netherlands) *(BuildSys '17)*. Association for Computing Machinery, New York, NY, USA, Article 8, 10 pages. https://doi.org/10.1145/3137133.3137148

[68] Xiaoying Yang, Jacob Sayono, Jess Xu, Jiahao Nick Li, Josiah Hester, and Yang Zhang. 2022. MiniKers: Interaction-Powered Smart Environment Automation. *Proc. ACM Interact. Mob. Wearable Ubiquitous Technol.* 6, 3, Article 149 (sep 2022), 22 pages. https://doi.org/10.1145/3550287

[69] Xiaoying Yang and Yang Zhang. 2021. CubeSense: Wireless, Battery-Free Interactivity through Low-Cost Corner Reflector Mechanisms. In *Extended Abstracts of the 2021 CHI Conference on Human Factors in Computing Systems* (Yokohama, Japan) *(CHI EA '21)*. Association for Computing Machinery, New York, NY, USA, Article 386, 6 pages. https://doi.org/10.1145/3411763.3451599

[70] Zhicheng Yang, Parth H Pathak, Yunze Zeng, Xixi Liran, and Prasant Mohapatra. 2016. Monitoring vital signs using millimeter wave. In *Proceedings of the 17th ACM international symposium on mobile ad hoc networking and computing*. 211–220.

[71] Zhicheng Yang, Parth H Pathak, Yunze Zeng, Xixi Liran, and Prasant Mohapatra. 2017. Vital sign and sleep monitoring using millimeter wave. *ACM Transactions on Sensor Networks (TOSN)* 13, 2 (2017), 1–32.

[72] Hui-Shyong Yeo, Gergely Flamich, Patrick Schrempf, David Harris-Birtill, and Aaron Quigley. 2016. Radarcat: Radar categorization for input & interaction. In *Proceedings of the 29th Annual Symposium on User Interface Software and Technology*. 833–841.

[73] AI Zakharov, LN Zakharova, and MG Krasnogorskii. 2018. Monitoring landslide activity by radar interferometry using trihedral corner reflectors. *Izvestiya, Atmospheric and Oceanic Physics* 54 (2018), 1110–1120.

[74] Youwei Zeng, Dan Wu, Jie Xiong, Enze Yi, Ruiyang Gao, and Daqing Zhang. 2019. FarSense: Pushing the range limit of WiFi-based respiration sensing with CSI ratio of two antennas. *Proceedings of the ACM on Interactive, Mobile, Wearable and Ubiquitous Technologies* 3, 3 (2019), 1–26.

[75] Dingtian Zhang, Jung Wook Park, Yang Zhang, Yuhui Zhao, Yiyang Wang, Yunzhi Li, Tanvi Bhagwat, Wen-Fang Chou, Xiaojia Jia, Bernard Kippelen, et al. 2020. OptoSense: Towards ubiquitous self-powered ambient light sensing surfaces. *Proceedings of the ACM on Interactive, Mobile, Wearable and Ubiquitous Technologies* 4, 3 (2020), 1–27.

[76] Jia Zhang, Yinian Zhou, Rui Xi, Shuai Li, Junchen Guo, and Yuan He. 2022. AmbiEar: MmWave Based Voice Recognition in NLoS Scenarios. *Proc. ACM Interact. Mob. Wearable Ubiquitous Technol.* 6, 3, Article 151 (sep 2022), 25 pages. https://doi.org/10.1145/3550320

[77] Yang Zhang, Yasha Iravantchi, Haojian Jin, Swarun Kumar, and Chris Harrison. 2019. Sozu: Self-Powered Radio Tags for Building-Scale Activity Sensing. In *Proceedings of the 32nd Annual ACM Symposium on User Interface Software and Technology* (New Orleans, LA, USA) *(UIST '19)*. Association for Computing Machinery, New York, NY, USA, 973–985. https://doi.org/10.1145/3332165.3347952

[78] Yang Zhang, Gierad Laput, and Chris Harrison. 2018. Vibrosight: Long-Range Vibrometry for Smart Environment Sensing *(UIST '18)*. Association for Computing Machinery, New York, NY, USA, 225–236. https://doi.org/10.1145/3242587.3242608

[79] Yang Zhang, Chouchang (Jack) Yang, Scott E. Hudson, Chris Harrison, and Alanson Sample. 2018. Wall++: Room-Scale Interactive and Context-Aware Sensing. In *Proceedings of the 2018 CHI Conference on Human Factors in Computing Systems* (Montreal QC, Canada) *(CHI '18)*. Association for Computing Machinery, New York, NY, USA, 1–15. https://doi.org/10.1145/3173574.3173847

[80] Mingmin Zhao, Tianhong Li, Mohammad Abu Alsheikh, Yonglong Tian, Hang Zhao, Antonio Torralba, and Dina Katabi. 2018. Through-wall human pose estimation using radio signals. In *Proceedings of the IEEE Conference on Computer Vision and Pattern Recognition*. 7356–7365.